Photonics with Ferroelectric Vortex Lattice

Ramaz Khomeriki[1)], Vakhtang Jandieri[2)], Koki Watanabe[3)],
Daniel Erni[2)], Douglas H. Werner[4)] and Jamal Berakdar[5)]
[(1] *Physics Department, Tbilisi State University, 3 Chavchavadze, 0128 Tbilisi, Georgia*
[(2)] *General and Theoretical Electrical Engineering (ATE), Faculty of Engineering, University of Duisburg-Essen and CENIDE - Center for Nanointegration Duisburg-Essen, D-47048 Duisburg, Germany*
[(3)] *Department of Information and Communication Engineering, Fukuoka Institute of Technology, 3-30-1 Wajirohigashi, Higashi-ku, Fukuoka 811-0295, Japan*
[(4)] *Department of Electrical Engineering, The Pennsylvania State University, University Park, PA 16802, USA*
[(5)] *Institut für Physik, Martin-Luther-Universität, Halle-Wittenberg, D-06099 Halle/Saale, Germany*

We consider a ferroelectric material consisting of a stack of a finite number of vortex-antivortex (clockwise-anticlockwise) arrays of the electric dipoles. A distance between the centers of vortex-antivortex along the x-axis is h and a distance between the nearest layers along the y-axis is equal to $2h$. Plane waves are impinging from free space with an angle of incidence φ. The proposed structure, which is invariant with respect to the z-axis, supports the propagation of both TE (E_z, H_x, H_y) and TM (H_z, E_x, E_y) waves with respect to both the y- and x-directions. A rotation of a single dipole $\mathbf{d}$ in the electromagnetic field $(\mathbf{E}, \mathbf{H})$ could be characterized by its three dimensional rotation angle $\boldsymbol{\alpha}$ dynamics as follows:

$$\hat{\mathbf{I}}\ddot{\boldsymbol{\alpha}} = \mathbf{d} \times \mathbf{E} + \mu_0 \boldsymbol{\ell} \times (\dot{\mathbf{d}} \times \mathbf{H}) \qquad (1)$$

where $\hat{\mathbf{I}}$ is a moment of inertia matrix, $\boldsymbol{\ell}$ is a radius vector connecting the centers of rotation and the electric dipole, the dot over $\mathbf{d}$ and $\boldsymbol{\alpha}$ means a derivative with respect to the time. In a linear limit, the term with a magnetic field $\mathbf{H}$ could be safely neglected (it is the second-order small term), thus in the considerations that follow we do not consider the second term at the right-hand side of (1). Presenting the dipole moment $\mathbf{d}$ as a sum of the static and time-dependent terms: $\mathbf{d} = \mathbf{d}_0 + \delta\mathbf{d}(t)$ and taking into account the fact that in the first-order approximation $\delta\mathbf{d} = \boldsymbol{\alpha} \times \mathbf{d}_0$, after linearizing (1) we obtain:

$$\hat{\mathbf{I}}\ddot{\delta\mathbf{d}} = -\mathbf{d}_0 \times (\mathbf{d}_0 \times \mathbf{E}). \qquad (2)$$

Note that $\mathbf{d}_0$ is lying in the xoy plane. Solving the second-order differential equation assuming that ω is an angular frequency of the plane electromagnetic waves, a relationship between the perturbed part of the electric dipole $\delta\mathbf{d}$ and the electric field $\mathbf{E}(x, y)$ in the grating layer is expressed in the following matrix equality: $\delta\mathbf{d} = \epsilon_0 \hat{\chi}\mathbf{E}$, where the electric susceptibility matrix reads as:

$$\hat{\chi} = \begin{pmatrix} -\frac{d_{0y}^2}{\epsilon_0 \omega^2 I_z} & \frac{d_{0y} d_{0x}}{\epsilon_0 \omega^2 I_z} & 0 \\ \frac{d_{0y} d_{0x}}{\epsilon_0 \omega^2 I_z} & -\frac{d_{0x}^2}{\epsilon_0 \omega^2 I_z} & 0 \\ 0 & 0 & -\frac{d_{0x}^2 + d_{0y}^2}{\epsilon_0 \omega^2 I_x} \end{pmatrix}. \qquad (3)$$

Here indices x, y or z are principle axis of rotatory motion, $I_x = I_y$, and ϵ_0 is the permittivity of free space.

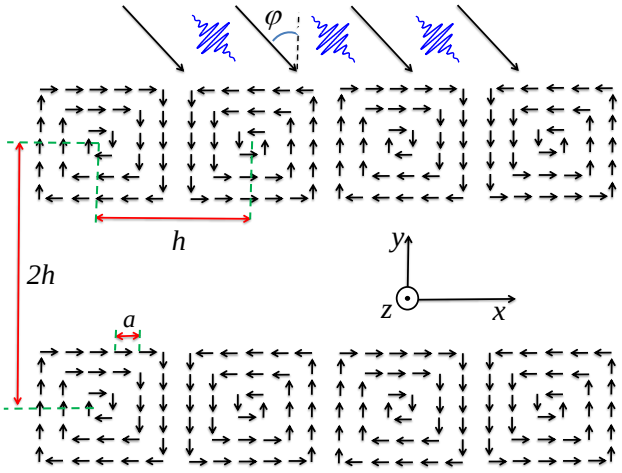

FIG. 1. Schematics for a vortex-antivortex ferroelectric lattice, where the distances between the centers of the vortices along the x and the y axes are h and $2h$, respectively. The structure has an uniform distribution of electric dipoles along the z direction and an angle of incidence of the plane electromagnetic waves is φ. A distance between the neighboring electric dipoles is denoted by a.

Note that the matrix elements are functions of x. It is important to emphasize that in the first-order approximation each element of the electric susceptibility matrix (3) is periodic function along the x-axis with a period h. In other words, in a linear regime the incident electromagnetic waves for both polarizations do not feel the electric dipole vortex-antivortex per unit cell and the problem is reduced to study an interaction of the incident waves with a single dipole vortex lattice (see Fig.1). Without loss of generality we also note that the electric dipoles are directed either along the x-axis or along the y-axis as it is shown in Fig. 1. Hence, the electric susceptibility matrix (3) has only diagonal nonzero components, since $\chi_{12} \sim d_{x0} d_{y0} = 0$. Obviously, the formalism presented in the work can be applied to the electric dipoles at arbitrary position when $\chi_{12} \neq 0$.

We start from the following normalized Maxwell's curl

equations:

$$\nabla \times \mathbf{E} = i\omega\mu_0\mathbf{H}, \qquad \nabla \times \mathbf{H} = -i\omega\left(\epsilon_0\mathbf{E} + \mathbf{P}\right) \tag{4}$$

where μ_0 is a magnetic permeability of the free space. The polarization vector $\mathbf{P}$ in (4) - the dipole moment per unit volume - is obtained by averaging $\delta\mathbf{d}$ and dividing it by a^3, where a is a characteristic distance between the dipoles as shown in Fig.1: $\mathbf{P} = \overline{\delta\mathbf{d}}/a^3$. The x, y and z components of the electromagnetic fields are pseudoperiodic functions of x with a period h and can be approximately expanded into a truncated Fourier series in the following form [...]:

$$\begin{bmatrix}\mathbf{E}(x,y)\\ \mathbf{H}(x,y)\end{bmatrix} = \sum_{n=-N}^{N}\begin{bmatrix}\mathbf{e}_n(y)\\ \mathbf{h}_n(y)\end{bmatrix} e^{i(k_x+2\pi n/h)x}, \tag{5}$$

where $k_x = (\omega/c)\sin(\varphi)$ and N is a truncation number associated with the Fourier series. In the numerical analysis that follows the truncation number N is taken as 8 to meet the energy conservation principle. Note that the n-th order Fourier coefficients are functions only of y. Expressing the y component of the electric and magnetic fields through the x and z components and replacing all the periodic functions with their Fourier series as in (5), Maxwell's equations can be transformed into the following coupled differential equations:

$$\frac{\partial}{\partial y}\begin{bmatrix}e_x\\ e_z\\ h_x\\ h_z\end{bmatrix} = i\frac{\omega}{c}\begin{bmatrix}\mathbf{U}_{11} & 0 & 0 & \mathbf{U}_{14}\\ 0 & 0 & \mathbf{U}_{23} & 0\\ 0 & \mathbf{U}_{32} & 0 & 0\\ \mathbf{U}_{41} & 0 & 0 & \mathbf{U}_{44}\end{bmatrix}\begin{bmatrix}e_x\\ e_z\\ h_x\\ h_z\end{bmatrix} \tag{6}$$

where

$$\mathbf{U}_{11} = -\mathbf{K}[\![\hat{\epsilon}_y]\!]^{-1}[\![\hat{\epsilon}_{xy}]\!] \quad \mathbf{U}_{14} = [\![\hat{\epsilon}_y]\!]^{-1}\mathbf{K^2} - \mathbf{I} \quad \mathbf{U_{23}} = \mathbf{I}$$
$$\mathbf{U}_{32} = -\mathbf{K}^2 + [\![\hat{\epsilon}_z]\!] \quad \mathbf{U}_{41} = -[\![\hat{\epsilon}_x]\!] + [\![\hat{\epsilon}_{xy}]\!][\![\hat{\epsilon}_y]\!]^{-1}[\![\hat{\epsilon}_{xy}]\!],$$
$$\mathbf{U}_{44} = -[\![\hat{\epsilon}_{xy}]\!][\![\hat{\epsilon}_y]\!]^{-1}\mathbf{K} \tag{7}$$

with a double bracket definition:

$$([\![\hat{\Upsilon}]\!])_{n,m} \equiv \frac{1}{h}\int_0^h \Upsilon(x)e^{-2i(n-m)\pi x/h}dx, \tag{8}$$

and $(\mathbf{K})_{n,m} = \delta_{n,m}(hk_x + 2\pi n)c/(h\omega)$, $\hat{\epsilon}_x = 1 + \hat{\chi}_{11}/a^3$, $\hat{\epsilon}_{xy} = \hat{\chi}_{12}/a^3$, $\hat{\epsilon}_y = 1 + \hat{\chi}_{22}/a^3$ and $\hat{\epsilon}_z = 1 + \hat{\chi}_{33}/a^3$, where the $\hat{\chi}$ matrix is defined in (3). Here $[\![\Upsilon]\!]$ is a square Toeplitz matrix generated by the Fourier coefficients of Υ with the (n,m) entries equal to Υ_{n-m}, a matrix in (6) is a $(8N+4)\times(8N+4)$ square matrix, $\mathbf{I}$ is the unit matrix and $\delta_{n,m}$ is the Kronecker's delta. The obtained coupled differential equation set is obviously separated into two independent sets that are connected with the TE and TM polarization cases. It is important to emphasize that a multiple scattering as between the layers within the unit cell, as well as between the arrays is described by solving for the scattering S-matrix which yields the relation between the incoming and outgoing wave amplitudes [**? ? ?**]. The reflection and transmission matrices for each layer are expressed through the eigenvectors and eigenvalues of the matrix in (6), whose components are given in (7). Since the reflection and transmission matrices for each layer are defined, the generalized reflection and transmission matrices matrix viewed from the uppermost region (region of incident wave) are calculated using a recursive algorithm [**? ? ?**] taking into account a phase shift between the adjacent layers along the y-axis.

The method based on the coupled differential equations presents an efficient numerical tool for the analysis of the arbitrary profiled gratings and fully characterizes the reflection and transmission properties for each space-harmonic and an interaction between them. However, to yield the explicit expressions for both bound and complex modes and study analytically the conditions necessary for formation of the passband and gap regions, we develop a fully independent approximate analytical method. Initial is a wave equation for the electric field inside the ferroelectric material, which is easily derived from (4):

$$\Delta\mathbf{E} - \boldsymbol{\nabla}\left(\boldsymbol{\nabla}\cdot\mathbf{E}\right) = -\omega^2\mu_0\hat{\epsilon}\mathbf{E} \tag{9}$$

where $\hat{\epsilon}(x,y) \equiv \mathrm{diag}[\epsilon_x, \epsilon_y, \epsilon_z]$ is a dielectric permittivity matrix. It is a diagonal matrix since the electric dipoles are directed only either along the x-axis or the y-axis. Since in the linear regime, the polarization densities are described by the rectangular functions periodic along both x-axis and y-axis with a period of h and $2h$, respectively, we expand the elements of dielectric permittivity matrix into the Fourier series keeping only the harmonics with wavenumbers $Q = 2\pi/h$ along the x-axis and $Q/2$ along y-axis, respectively. It could be considered as a rough approximation, however, as we will see below, it qualitatively well describes the dispersion characteristics of the modes and the results agree well with the results obtained based on the rigorous coupled-wave method. As a result, the elements of the dielectric permittivity matrix can be written in the following form:

$$\epsilon_x = \epsilon_0 - \tfrac{\epsilon_0\kappa^2}{4\omega^2}\left[1 + \tfrac{4}{\pi}\cos\tfrac{Qy}{2} + \dots\right]\left[1 + \tfrac{4}{\pi}\cos Qx + \dots\right]$$
$$\epsilon_y = \epsilon_0 - \tfrac{\epsilon_0\kappa^2}{4\omega^2}\left[1 + \tfrac{4}{\pi}\cos\tfrac{Qy}{2} + \dots\right]\left[1 - \tfrac{4}{\pi}\cos Qx - \dots\right]$$
$$\epsilon_z = \epsilon_0 - \tfrac{\epsilon_0(\kappa')^2}{2\omega^2}\left[1 + \tfrac{4}{\pi}\cos\tfrac{Qy}{2} + \dots\right] \tag{10}$$

where $Q \equiv 2\pi/h$, $\kappa \equiv \sqrt{d_0^2/(a^3 I_z\epsilon_0)}$ and $\kappa' \equiv \kappa\sqrt{I_z/I_x}$ characterize dipolar interactions.

Wave equation (9) has a simple form in case of TE polarization, since ϵ_z defined by (10) is homogeneous along the x-axis and only varies periodically along the y-axis with a corresponding harmonic wavenumber $Q/2$. In other words, under given polarization the electromagnetic wave does not feel the vortex structure along the x-axis and the scattering problem is reduced to a simple problem of multiple interaction between the stripes separated by a free space along the y-axis (see Figs.2a and

2b). Thus, (9) can be written in Fourier representation in the following form:

$$\left[\frac{\omega^2}{c^2}-\frac{(\kappa')^2}{2c^2}-k_x^2-k_y^2\right]E^z_{\mathbf{k}}=\frac{(\kappa')^2}{\pi c^2}\left[E^z_{\mathbf{k}+\mathbf{Q_y}}+E^z_{\mathbf{k}-\mathbf{Q_y}}\right]. \tag{11}$$

where $\mathbf{k}=(k_x,k_y)$ is a wavevector characterizing the Bloch modes, $\mathbf{Q_y}$ is a wavenumber related to the periodicity of the lattice along the y axis: $\mathbf{Q_y}=(0,Q/2)$, and $(\kappa')^2/\pi$ is a respective coupling constant between the different Bloch modes. It should be noted that for the frequencies $\omega\lesssim Qc/4$, the terms on the right side of (11) could be safely neglected and the dispersion relation can be written in the following simple form:

$$\omega=c\sqrt{k_x^2+k_y^2+(\kappa')^2/c^2} \tag{12}$$

From (12) it follows that in case of TE polarization a bandgap is formed when $\omega<\kappa'/\sqrt{2}$. Note that we do not consider the interactions between the electric dipoles, which correspond to the frequencies in the vicinity of κ and κ'.

At the higher frequencies $\omega^2\gg\kappa^2$, $(\kappa')^2$ and contribution of κ and κ' can be neglected compared to the excitation frequencies ω.

Thus, in the higher frequency range, particularly when $Qc/4\lesssim\omega\lesssim Qc/2$, we have two intersecting dispersion curves:

$$\omega(\mathbf{k})=c\sqrt{k_x^2+k_y^2},\quad \omega(\mathbf{k}-\mathbf{Q_y})=c\sqrt{k_x^2+(k_y-Q/2)^2} \tag{13}$$

A region of intersection is associated with the frequency range ω where k_y acquires an imaginary part (a reflection peak appears in this frequency region). For more detailed analysis the terms at the right side of (11) should be taken into account and the coupled equations for the above two modes with the wavenumbers $\mathbf{k}$ and $\mathbf{k}-\mathbf{Q_y}$ can be written in the following form:

$$\begin{aligned}\left[\frac{\omega^2}{c^2}-k_x^2-k_y^2\right]E^z_{\mathbf{k}}&=\frac{(\kappa')^2}{\pi c^2}E^z_{\mathbf{k}-\mathbf{Q_y}}\\ \left[\frac{\omega^2}{c^2}-k_x^2-(k_y-Q/2)^2\right]E^z_{\mathbf{k}-\mathbf{Q_y}}&=\frac{(\kappa')^2}{\pi c^2}E^z_{\mathbf{k}}\end{aligned} \tag{14}$$

Then one can easily deduce that at a point of intersection $\omega^P=cQ/(4\cos\varphi)$, a real part of the transverse wavenumber is $k_y^P=Q/4$. Moreover, from (13) we can accurately calculate a full width $\Delta\omega^P$ and a height G^P of the imaginary part of k_y:

$$\Delta\omega^P=\frac{4(\kappa')^2}{\pi\cos(\varphi)cQ},\quad G^P=\frac{2(\kappa')^2}{\pi cQ} \tag{15}$$

The analytical approximate method very well describes the coupling mechanism of the electromagnetic waves

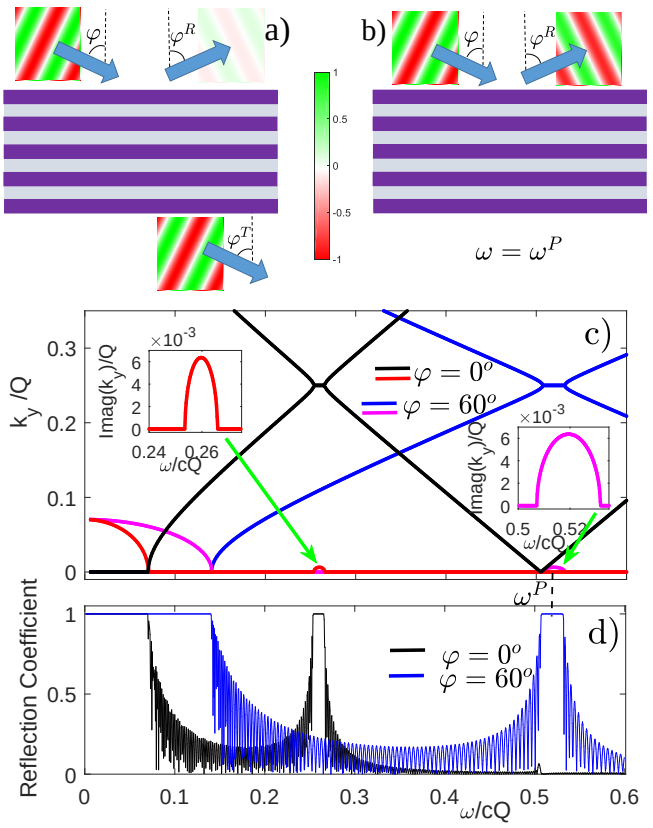

FIG. 2. Scattering properties of TE (E_z, H_x, H_y) electromagnetic field coupled with the vortex-antivortex lattice (Fig.1). As noted in the text, the TE field feels only the lattice inhomogeneities along the y axis, that is why we display the lattice as horizontal stripes in graphs a) and b), where the incident angle is $\varphi=60^o$. Field distributions of the reflected and transmitted waves are given at: (a) the frequency outside the gap region; (b) at the frequency $\omega=\omega^P$ in the gap region. The latter is calculated from (15). Graph c) displays dispersion curves in case of normal incidence $\varphi=0^o$ and oblique incidence $\varphi=60^o$, which follow from the Bloch mode analysis of (11). In the crossing points one observes the imaginary parts of k_y corresponding to the complete stopband region (a complete reflection of the field in the respective frequency range), which is confirmed by rigorous coupled-wave method (4)-(8) and the result of the reflection coefficient is shown in graph d). A number of vortex-antivortex stripes along the y-axis is equal to 100.

with the arrays formed by the vortex-antivortex electric dipoles. The results are compared with those obtained based on the rigorous coupled-wave method and are presented in Fig.2. Graph c) displays the dispersion curves at the normal $\varphi=0^o$ and at the oblique incidence $\varphi=60^o$ based on the Bloch mode analysis of (11). In the vicinity of the crossing points we get the imaginary parts of k_y corresponding to the complete stopband region (red lines in Fig.2c). A complete reflection of the field is observed in these frequency ranges for both angles of incidence and it is confirmed by rigorous coupled-wave

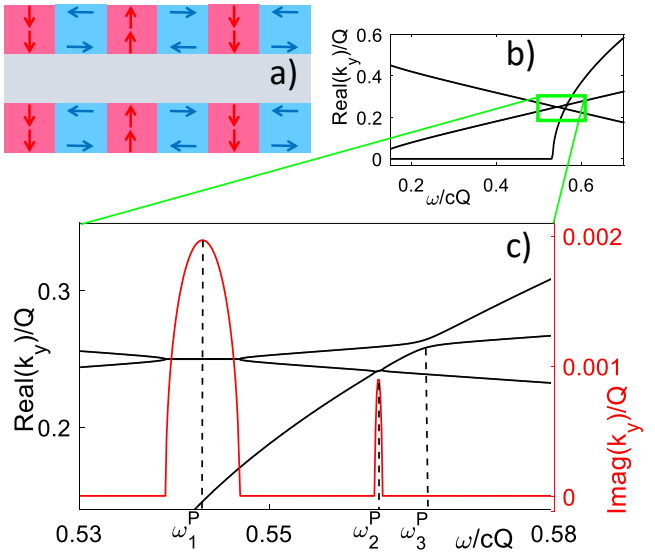

FIG. 3. Scattering properties of TM (H_z, E_x, E_y) electromagnetic field coupled with the vortex-antivortex lattice (Fig.1). a) Schematics of vortex-antivortex lattice described by the dielectric permittivity matrix (10); b) dispersion curves calculated from (14) at an angle of incidence $\varphi = 62^o$; c) enlarged view of the dispersion curves' crossing points (green square in graph b)). At two crossing points, namely at ω_1^P and ω_2^P, k_y is a complex value, whereas at $\omega \simeq \omega_3^P$ an avoided crossing of dispersion curves is observed and k_y is a pure real value. A number of vortex-antivortex lattice along the y-axis is equal to 100.

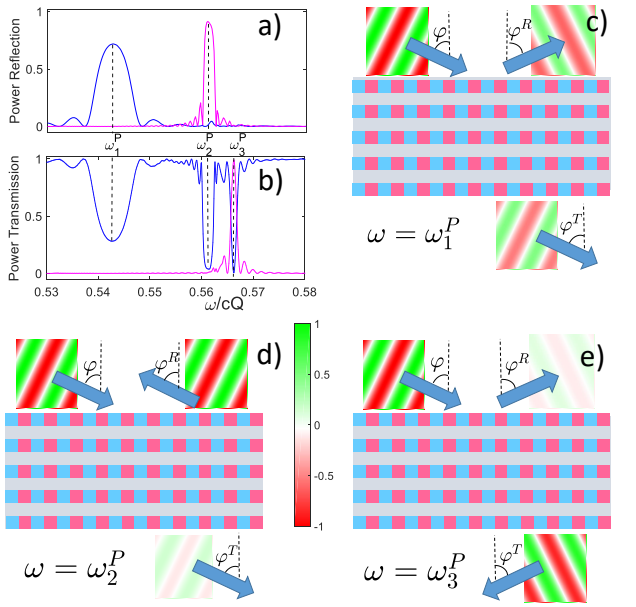

FIG. 4. a) A dependence of the reflected and b) transmitted powers of the TM wave versus the normalized angular frequency ω/cQ calculated based on the rigorous coupled-wave method (4)-(8). The angle of incidence is $\varphi = 62^o$. Blue line corresponds to the reflection and transmission of the plane waves having a positive k_x (propagating 0th space-harmonic), whereas a violet line corresponds to the reflection and transmission of the plane waves with negative k_x (propagating -1st space-harmonic) due to the presence of the vortex-antivortex lattice along the x-axis. Other three graphs display schematically the reflection and transmission processes at three frequencies corresponding to the crossing points of the branches illustrated in Fig.3.

method (4)-(8) as demonstrated in graph d). Field distributions of the reflected and transmitted waves are also demonstrated in Fig.2a and 2b at: (a) the frequency outside the gap region; (b) at the frequency $\omega = \omega^P$ in the gap region. A number of vortex-antivortex stripes along the y-axis is equal to 100.

As for the TM polarization, the coupled equations for the electric field components can be written in the following form:

$$(\frac{\omega^2}{c^2} - k_y^2)E^x_{\mathbf{k}} + k_x k_y E^y_{\mathbf{k}} = \sum_s (\kappa^x_s/c)^2 E^x_{\mathbf{k}+\mathbf{Q_s}} \quad (16)$$

$$(\frac{\omega^2}{c^2} - k_x^2)E^y_{\mathbf{k}} + k_x k_y E^x_{\mathbf{k}} = \sum_s (\kappa^y_s/c)^2 E^y_{\mathbf{k}+\mathbf{Q_s}}$$

where $\mathbf{Q_s}$ includes the wavenumbers $\pm\mathbf{Q_y} \equiv (0, \pm Q/2)$, $\pm\mathbf{Q_x} \equiv (\pm Q, 0)$ and their linear combination, while κ^x_s and κ^y_s are respective Bloch modes' coupling constants proportional to κ. The dispersion characteristics for the frequencies $\omega \lesssim cQ$ are described by three coupled branches characterized by the wavenumbers $\mathbf{k}$, $\mathbf{k} - \mathbf{Q_y}$ and $\mathbf{k} - \mathbf{Q_x}$. For the first two branches the coupling constants are $\kappa^x_1 = \kappa^y_1 = \kappa/2\pi$, for the first and the third branches the coupling constants are $\kappa^x_2 = -\kappa^y_2 = \kappa/2\pi$ and the last two branches are connected by the coupling constants $\kappa^x_1 = -\kappa^y_1 = \kappa/\pi^2$. In the absence of the coupling effects, (13) should be supplemented by the dispersion relation of the third mode $\omega(\mathbf{k} - \mathbf{Q_x}) = c\sqrt{(k_x - Q)^2 + k_y^2}$. Thus, we get the three dispersion curves:

$$ck_y = \omega\cos\varphi, \qquad ck_y = Q/2 - \omega\cos\varphi, \quad (17)$$
$$ck_y = \sqrt{\omega^2\cos^2\varphi + 2cQ\omega\sin\varphi - c^2Q^2}$$

Their intersection points can be easily found from (17):

$$\omega_1^P = \tfrac{cQ}{4\cos\varphi} \quad \omega_2^P = \tfrac{5cQ}{4(\cos\varphi + 2\sin\varphi)} \quad \omega_3^P = \tfrac{cQ}{2\sin\varphi}. \quad (18)$$

Analyzing the coupling behaviour of the dispersion curves of these three modes, we may conclude that: transverse wavenumbers k_y are complex values at the intersection points ω_1^P and ω_2^P corresponding to the intersection of the first two branches and the second and the third branches, respectively. At an intersection point ω_3^P of the first and the third curves, we get an avoiding crossing and k_y is a pure real value. This means that at ω_3^P a transmission of $\mathbf{k} - \mathbf{Q_x}$ mode will be observed irrespective of the thickness of the sample, whereas the behaviour of $\mathbf{k}$ and $\mathbf{k} - \mathbf{Q_x}$ modes near the intersection

points at ω_1^P and ω_2^P strongly depends on the thickness of the sample.

Dispersion curves and the enlarged view of their points of intersections at an angle of incidence $\varphi = 62^o$ are shown in Figs.3b and 3c. The first crossing point that appears at ω_1^P is associated with two branches both having an equal wavenumber component k_x. Thus, we expect that $\varphi^R = \varphi^T = \varphi$, where φ^R and φ^T are the angles of reflection and transmission, respectively. The latter is confirmed numerically by the rigorous coupled-wave method and demonstrated in Figs.4a-4c. For two other points of intersections appearing at ω_2^P and ω_3^P, we have both k_x and $k_x - Q$ wavenumber components excited. Reflection and transmission angles of the branches associated with $k_x - Q$ are simply calculated as $\sin\varphi^{R,T} = c(k_x - Q)/\omega = \sin\varphi - cQ/\omega$ and after inserting here (18) at the crossing points $\omega = \omega_2^P$ and $\omega = \omega_3^P$, we get the following expressions:

$$\sin\varphi_2^{R,T} = -\frac{4\cos\varphi + 3\sin\varphi}{5}, \quad \sin\varphi_3^{R,T} = -\sin\varphi. \quad (19)$$

A comparison with the rigorous coupled-wave method is shown in Fig.4d and 4e. An agreement between the results is very good. The analysis gives a full picture of the coupling behaviour of the electromagnetic waves with the vortex-antivortex of electric dipole arrays.